



Assessment of ecophysiology of lake shore reed vegetation based on chlorophyll fluorescence, field spectroscopy and hyperspectral airborne imagery

Dimitris Stratoulas^{a,b,*}, Heiko Balzter^b, András Zlinszky^a, Viktor R. Tóth^a

^a Balaton Limnological Institute, Hungarian Academy of Sciences, Klebelsberg Kuno u. 3, Tihany H-8237, Hungary

^b University of Leicester, Centre for Landscape and Climate Research, Bennett Building, University Road, Leicester LE1 7RH, U.K.

ARTICLE INFO

Article history:

Received 30 December 2013

Received in revised form 10 April 2014

Accepted 30 May 2014

Available online 19 July 2014

Keywords:

Spectral indices

Chlorophyll fluorescence

Hyperspectral

Ecophysiology

Reed die-back

Airborne remote sensing

ABSTRACT

Since the beginning of the 1960s an escalating deterioration of reed beds in parts of Europe has been often observed. Hence, the 'reed die-back' as it was later named, has been a phenomenon of great scientific interest and concern to conservationists worldwide and intensively studied by field ecologists. Imaging spectroscopy has frequently been employed for vegetation mapping, but this paper is the first explicit analysis of the spectral information content for reed and an assessment of the potential for detecting the areas affected by the reed die-back syndrome using hyperspectral data at the near infrared and the chlorophyll absorption spectral regions. Leaf reflectance spectra and photophysiological information were acquired using a Hand-Held ASD spectroradiometer, a portable fluorometer and a chlorophyll metre *in-situ* concurrently from leaf samples along a transect perpendicular to the lake shore of Central Europe's largest inland lake in terms of area, Lake Balaton in Hungary. A strong correlation between narrowband spectral indices and chlorophyll fluorescence parameters indicates the potential of hyperspectral remote sensing in assessing plant stability. Canopy hyperspectral data were collected from an airborne AISA Eagle sensor (400–1000 nm). An application of the findings from the field data analysis to airborne hyperspectral imagery reveals important information about reed condition at the study area. $Y(II)$ values, regarded as a proxy of photosystem activity, have been calculated from high R^2 combination of spectral ratio 612/516 representing F_s and 699/527 representing F_m' . ETR values are estimated based on the calculated $Y(II)$ and the spectral ratio 463/488 for Photosynthetically Active Radiation. This research underpins the development of methods for the spectral discrimination of reed patches affected by stress caused by environmental conditions, and subsequently the reed die-back syndrome. A comparison with empirical vegetation indices from the literature shows significantly higher R^2 values of the proposed indices for the specific application. We recommend spectral indices at leaf level for evaluating reed ecological status based on spectroscopic data to support the identification of affected vegetation patches and present R^2 maps that can aid the selection of indices tailored to specifications of remote sensors.

© 2014 The Authors. Published by Elsevier Inc. This is an open access article under the CC BY license (<http://creativecommons.org/licenses/by/3.0/>).

1. Introduction

Phragmites australis (Cav.) Trin. ex Steudel (common reed) is one of the most widespread vascular plants on the Earth, growing in all continents except Antarctica (Tucker, 1990). It is a tall rhizomatous perennial grass (Haslam, 1969) typically encountered in wetland environments and more frequently in land–water interface zones (Tucker, 1990). Acting as a buffer zone between terrestrial and aquatic ecosystems (Brix, 1999), it holds an important role as the key species of temperate wetlands and delivers valuable ecosystem services such as maintaining

the shore stability (Engloner, 2009). Since the beginning of the 1960s a widespread, non-reversible and abnormal retreat of reed areas has been observed in parts of Europe (Brix, 1999; Van der Putten, 1997). The phenomenon was first reported 60 years ago from Hürlimann (1951), cited in Ostendorp (1989) and on Lake Balaton from Tóth et al. (1961). Since then an increasing scientific interest and environmental concern has been raised. Typical indicative expressions reported include reduced plant height, weaker culms, abnormal rhizomes, formation of clumps (Fogli et al. 2002), gradual thinning, and eventually natural degeneration and retreat from relatively deep water (Van der Putten, 1997). These factors signifying an abrupt reduced stability are collectively reported in the literature as the 'reed die-back syndrome'. However, contrary to the typical stress manifestation in the leaf structure of most plants, identification of die-back conditions is not

* Corresponding author at: Balaton Limnological Institute, Klebelsberg Kuno u. 3, Tihany H-8237, Hungary. Tel.: +36 703483250.

E-mail address: dimitris.stratoulas@gmail.com (D. Stratoulas).

straightforward when using macroscopic visual assessment especially at an early stage, because of the connection of individual shoots by underground rhizomes allowing sharing of nutrients. Thus, while the entire plant may be in a state of die-back, the leaves do not necessarily show typical signs of deterioration.

Vegetation photosynthetic systems are very sensitive to environmental induced stress. The first exhibition of leaf stress, preceding morphometric changes, is reduced photosynthetic performance and more specifically damage the Photosystem-II (PSII) (Maxwell & Johnson, 2000) which is quantitatively correlated to chlorophyll fluorescence yield. Thus photochemical parameters measured *in-situ* can provide an early diagnostic indicator of plants' stress and it is a well-studied fact that production of plants can be easily and non-intrusively estimated by chlorophyll fluorescence. Photochemical parameters usually relate to the apparent (F_s) and maximum (F_m') values of fluorescence yield (Maxwell & Johnson, 2000). Genty et al. (1989) proposed a widely used formula to estimate changes in quantum yield defined as:

$$Y(II) = \frac{\Delta F}{F_m'} = \frac{F_m' - F_s}{F_m'} \quad (1)$$

$Y(II)$ represents the ratio of open to close PSII centres at given irradiance, which is the proportion of energy used between photosynthesis and other processes, relating directly to plant stress. More specifically it is a measurement of the transfer of electrons between photosystems within the process of photosynthesis. Since during photosynthesis 4 electrons must be transported for every assimilated CO_2 molecule, $Y(II)$ represents the potential possible driving force of photosynthesis. Therefore it relates to net photosynthesis, however in a curvilinear way because unknown stress factors, light dissipation and others might influence $Y(II)$ values. Another factor related to production of photosynthesis is the Electron Transport Rate (ETR) which is defined as

$$ETR = \frac{\Delta F}{F_m'} \times PAR \times AF \times 0.50 \quad (2)$$

where 0.5 accounts for distributing the energy between PSI and PSII and AF is the absorption factor for the leaves. ETR within the PSII can be measured by PAM fluorometry and translates directly into production of photosynthesis, a parameter which provides significantly enhanced information in comparison to the photosynthetic activity at the given environmental conditions and time. When measured in a context of a correct methodological approach, it allows to measure both potential and apparent photosynthetic activity and photosynthetic efficiency. The comparison of these parameters could reveal the processes within the PSII, where the electron transport was decoupled, which sheds light on the effect of the apparent environmental conditions on the process of photosynthesis. For a comprehensive explanation of chlorophyll fluorescence the reader is referred to Krause and Weis (1991) and Baker (2008).

Remote sensing applications for the mapping of reed condition in Europe have been reported in the literature but their function so far has been limited to a tool for assessing the distribution of vegetation species and sometimes the plant health categorically; however quantification of reed stress physiological indicators has not been attempted. For example, Bresciani et al. (2009) used remotely sensed data to monitor reed vigour represented by the Leaf Area Index (LAI) in three environmentally sensitive Italian lakes. Liira et al. (2010) estimated the macrophytic expansion in a eutrophic Lake based on a Landsat TM and ETM+ time series. Hunter et al. (2010) mapped the distribution of macrophytes in a clear British shallow lake. Onojeghuo and Blackburn (2011) demonstrated the synergistic use of hyperspectral and Light Detection and Ranging (LiDAR) data for mapping reed bed habitats and Bresciani et al. (2011) estimated the LAI from field and satellite data in the context of reed conservation. Lately, Zlinszky et al. (2012) used discrete return LiDAR to categorize aquatic vegetation and stressed reed in Lake Balaton, Hungary and Villa et al. (2013)

presented an approach to monitor reed conservation status of Lake Garda in Italy with a variety of remotely sensed datasets. Remote sensing inherently has the capacity of species distribution mapping in lake-shore environments, however, macrophyte physiological status has not been yet investigated thoroughly from a remote sensing perspective. Despite the fact that chlorophyll fluorescence is one of the most powerful stress detection methods in plant ecophysiology (Maxwell & Johnson, 2000), coupling with remote sensing has not yet been widely examined.

Attempts to relate leaf spectral information with several physiological and morphological parameters have been widely reported in the literature, such as with chlorophyll, nitrogen, water or biomass content and leaf density. While some of these parameters have been proven to correlate highly with spectral indices, chlorophyll fluorescence provides significantly more information on the photosynthetic activity of plants than the aforementioned parameters.

The coupling between physiological parameters and spectral information is often established by building indices in the form of mathematical formulae integrating spectral bands. These spectral indices are typically developed on the basis of empirical observations or experimental processes as a proxy to vegetation characteristics. For instance, Zarco-Tejada et al. (2001) propose that the ratio of the reflectance of 750 nm and 710 nm is a good indicator of chlorophyll content at leaf level. Gitelson and Merzlyak (1996) suggest that the indices R_{750}/R_{550} and R_{750}/R_{700} are highly proportional (correlation $R^2 > 0.95$) to chlorophyll concentration in leaves. In a similar manner Vogelmann et al. (1993) propose R_{740}/R_{720} as well as the ratio of first derivative values D_{715}/D_{705} . Stagakis et al. (2010) in a thorough investigation of chlorophyll indices suggest that mNDVI (Sims & Gamon, 2002), PSRI (Merzlyak et al. 1999) and SIPI (Peñuelas et al. 1995) perform well in chlorophyll estimation. Finally, Thenkabail et al. (2000) present a study on the relationship between vegetation indices and agricultural crop characteristics where they suggest that remarkably strong relationships are found in specific narrow bands.

This paper presents the first investigation of the potential of hyperspectral remote sensing for characterizing the ecophysiological status of reed in a lake shore environment based on fluorometric *in-situ* measurements. Imaging spectroscopy has lately been emerging as a promising technique for vegetation-related applications and scientific improvements are needed to sustain the potential for advancement in this field (Thenkabail et al. 2012). Lake Balaton, Hungary is the largest (596 km²) and a relatively shallow (mean water depth 3.25 m) freshwater lake in Central Europe (Virág, 1997). It encompasses a total area of ca. 11 km² of reed stands stretching along 112 km of the 254 km of the shoreline, with the majority situated on the north shore, part of which has suffered intense reed die-back from 1970s onwards (Kovács et al., 1989). In this study we attempt to assess the spectral signatures of reed samples of different inundation levels from a perpendicular transect at a relatively stable basin of the lake. We used statistical analysis to quantify the association between chlorophyll fluorescence kinetics and hyperspectral signatures of reed leaves. We identified spectral indices correlating significantly to fluorescence yield, and thus vegetation stability. An application of lake-shore vegetation status assessment based on hyperspectral airborne collected imagery demonstrates the potential of remote sensing for reed stability quantification.

2. Materials and methods

In-situ and airborne datasets were collected in the Kerekedi bay (46° 58' 2.84" N, 17° 55' 4.34" E), the easternmost mesotrophic basin of Lake Balaton, Hungary (Fig. 1). The field measurements were collected on August 14th, 2012 at the climax of the growing period in the area of study and under clear sky conditions between 11:00 and 13:00 local time (Central European Time). Fluorescence, chlorophyll and hyperspectral measurements were recorded concurrently from the middle of leaf samples collected along a transect aligned perpendicular to the

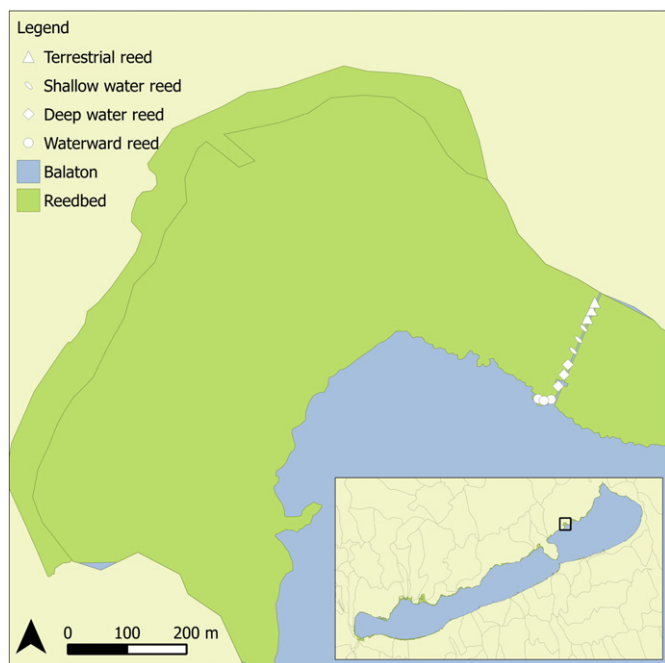


Fig. 1. Relative position of Kerekedi Bay (46° 58' 2.84" N, 17° 55' 4.34" E) in Lake Balaton and location of sampling points.

lake shore at the north-eastern part of the bay. The sampling area was divided into four categories according to the level of inundation of the reed stand, namely terrestrial, shallow water, deep water and water-front regions. Water level is a factor representing different environments within the reed bed in our study, and its fluctuation has been an important aspect as reported in the literature (Paillisson & Marion, 2011). We collected measurements at 23, 55, 27 and 17 points of the transect respectively for the 4 categories. In the terrestrial part of the transect sediment was not covered with water, in the shallow part the sediment was covered with up to 15 cm of water, at the deep part of the transect the plants were covered with more than 15 cm of water, while reed at depth of more than 140 cm and up to 5 m distance to the reed-water boundary was considered as the waterfront category. The latter is receiving higher environmental pressure from wind, wave mechanical damage, litter accumulation and manoeuvring from fishing boats docking between the reed stands.

2.1. Fluorescence and chlorophyll measurements

In-situ measurements were obtained along the transect at Kerekedi Bay (Fig. 1). The reed bed was covered by a stand of monospecific *Phragmites*, although at the terrestrial part *Carex* sp. was co-dominant. The measurements were performed at the middle third of the youngest fully matured leaves of *Phragmites* in full sunlight conditions. Leaf chlorophyll content was estimated by a SPAD-502 chlorophyll metre (Konica Minolta, Inc., Japan). Light adapted chlorophyll fluorescence data were acquired on site using a PAM-2500 fluorometer (Heinz Walz GmbH, Germany). For each sample we measured the apparent (F_s) and maximum (F_m') values of fluorescence in the light-adapted state as well as the Photosynthetically Active Radiation (PAR) (measured in $\mu\text{mol quanta m}^{-2} \text{s}^{-1}$). Additionally, the effective quantum yield of photochemistry, i.e. the fraction of absorbed photons used by the photochemical systems ($Y(\text{II})$) and the ETR were calculated on the basis of Eqs. (1) and (2). AF is the absorption factor for the leaves and in this study has been assumed a constant equal to $\text{AF} = 0.86$ for the following reasons; first, the samples are collected from a single species of the same age in a monospecific reed stand. Furthermore the age

difference between the leaf samples (of plants of the same age) due to the apical growth of *Phragmites* has been minimized by selecting only the apical first fully mature leaf. Last but not least, chlorophyll content according to the finding of our statistical analysis (Fig. 3) has a rather constant distribution across the whole dataset.

2.2. In-situ hyperspectral measurements

Ground-based hyperspectral measurements were recorded concurrently using a Hand-Held ASD portable FieldSpec 2 spectroradiometer (Analytical Spectral Devices Inc., USA). The instrument records radiation intensity in 750 consecutive channels at the spectral domain 325–1075 nm with a resolution of less than 3 nm at 700 nm. Leaf reflectance values were acquired through a leaf clip attached to the device with an optical fibre. The source of light was integrated in the leaf clip and the black reference panel on the opposing side was used to calibrate the instrument for the reflectance values. For each leaf sample 10 measurements were taken at 544 ms integration time from the same point and averaged.

2.3. Airborne hyperspectral measurements

A wide-ranging dataset is available for the whole Lake Balaton shore comprising of airborne imagery and *in-situ* measurements. The former have been collected in summer 2010 during a European Facility for Airborne Research (EUFAR) campaign undertaken by the Airborne Research and Survey Facility (ARSF, Gloucester, U.K.). It consists of concurrently recorded hyperspectral, LiDAR and aerial photography data covering the whole lake shore (Zlinszky et al. 2011). The hyperspectral imagery was collected from an airplane-mounted Specim's AISA dual system (Spectral Imaging Ltd., Finland) incorporating sensors Eagle and Hawk. In this study we employ an image from Eagle sensor acquired over the Kerekedi bay collected on August 26th, 2010 at 15:17 Coordinated Universal Time. The apparent position of the sun at the time of image acquisition is defined by Altitude = 23.47 and Azimuth = 259.77 as calculated by the NOAA Solar calculator (url: <http://www.esrl.noaa.gov/gmd/grad/solcalc/>). The angle between the line of sight of the sensor and the zenith is 180° since AISA is a nadir looking instrument. The Eagle hyperspectral sensor was able to acquire narrow-band measurements in the spectral domain 400–1000 nm at 253 consecutive channels with a full width at half maximum between 2.20 and 2.44.

The image was first pre-processed by applying radiometric calibration and geometric registration on a 1 m grid scale. Atmospheric correction was implemented in the ENVI module FLAASH, based on a modified version of the MODTRAN4 radiation transfer code. Atmospheric correction is necessary in this application since there exists the need to convert the at-sensor radiance values to radiance at-target in order to allow fitting the results derived from the field data to the airborne image. We employed the mid-latitude summer atmospheric model and retrieved the water content from the 820 nm channel. The CO_2 mixing ratio was set to 404 ppm. No predefined aerosol model was used since this requires information from the 2100 nm channel which is outside the dataset range. The aerosol amount was estimated by the visibility which was set to 50 km in agreement with the atmospheric conditions on the day of the acquisition and confirmed by the local METAR report. Overall the atmospheric correction provided typical spectral responses for the vegetation in the image. No artefacts were apparent, due to the clear sky conditions at the time of image acquisition and the lack of open water absorbing bodies around the mesotrophic Kerekedi bay.

2.4. Methodology

We first investigated the spectral curves of the inundation categories and estimated to what degree the spectral response differentiates. The Tukey–Kramer Test (Pairwise Comparisons for One-Way Layout

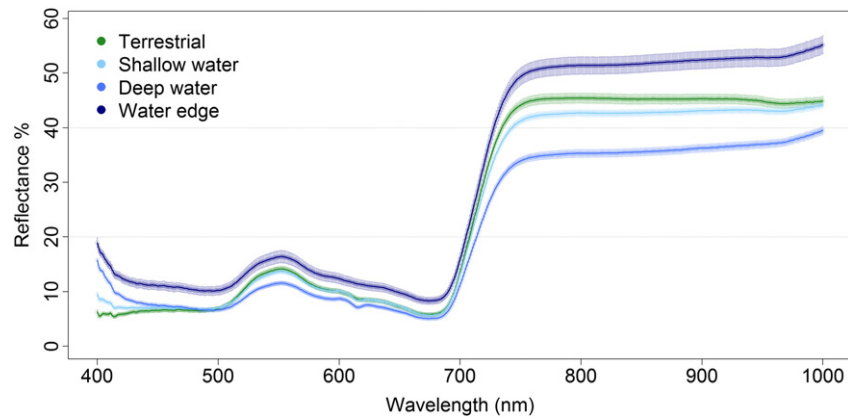


Fig. 2. Mean reflectance spectra and 95% confidence intervals for the mean of *Phragmites australis* leaf samples collected from the terrestrial, shallow water, deep water and waterfront of reed stand in Kerekedi Bay, Lake Balaton.

Design) was used also to compare the photophysiological data collected from the fluorometer and the CHL metre for each category. Thereafter, the methodology was based on the characterization of the physiological status of reed from the field spectroradiometer data and subsequently applying this method to the airborne data. The approach was

established partly by taking as guidance the study presented by Inoue et al. (2012) on correlating hyperspectral data with canopy nitrogen content in paddy rice for diagnostic mapping. The collected hyperspectral *in-situ* data were exported using the bundled software ViewSpec Pro 6.0 (Analytical Spectral Devices Inc., USA) and the main processing was

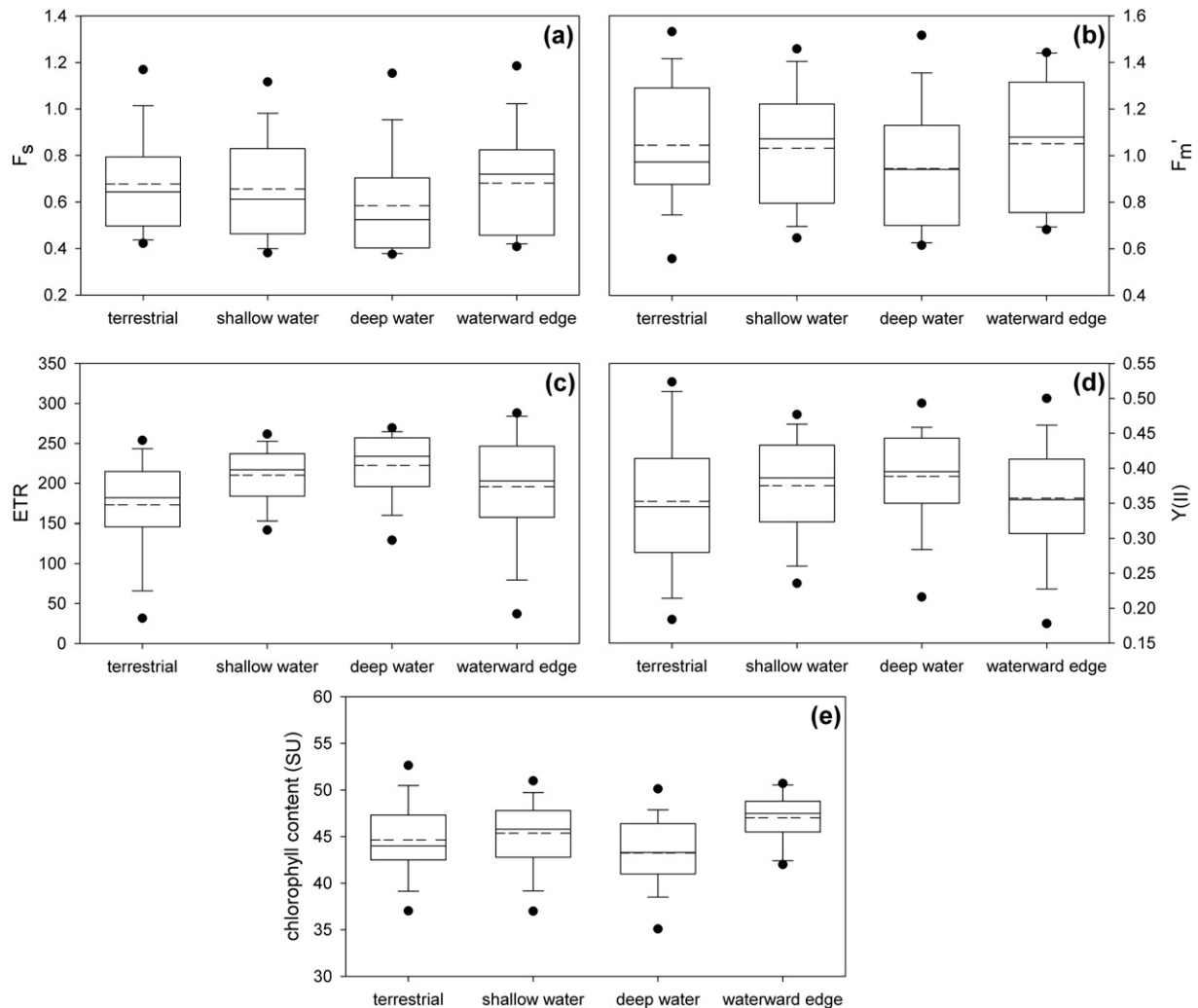


Fig. 3. Changes of: (a) F_s , (b) F_m' , (c) ETR, (d) $Y(II)$ and (e) CHL content of leaves of *Phragmites australis* at the terrestrial, shallow water, deep water and waterfront of the reed bed at the study site. $n = 27-55$. The comparison was performed using the Tukey–Kramer Test (Pairwise Comparisons for One-Way Layout Design). Boxes encompass the 25% and 75% quartiles of all the data for each specific part of the studied area. The central solid line represents the median, while the dashed line represents the average, bars extend to the 95% confidence limits, and dots represent outliers.

implemented in the R programming language (R Core Team, 2013). In the raw data, the marginal ranges 325–400 nm and 1000–1075 nm from each spectrum were removed due to noise effects. While discrimination analysis can be performed in order to select the optimum bands, in this study we concentrate on deriving the complete combination of spectral indices between all channels. The aim of spectral indices is to construct a mathematical combination of spectral band values for enhancing the information content in regard to the parameter under study. Many of the indices found in the literature are formed as a Ratio Spectral Index (RSI) of one band to another such as:

$$RSI(i, j) = \frac{R_i}{R_j} \quad (3)$$

where R_i and R_j are the intensity values for bands i and j respectively. The Normalised Difference Spectral Index (NDSI) is another transformation frequently used defined as:

$$NDSI(i, j) = \frac{R_i - R_j}{R_i + R_j} \quad (4)$$

A vegetation-specific representation of NDSI is the Normalised Difference Vegetation Index (NDVI) applied on a near-infrared and a red channel as reported first by Rouse et al. (1974).

RSI and NDSI for the hyperspectral spectra were calculated from complete combinations of the available bands, as in similar studies (e.g. Inoue et al., 2012; Stagakis et al., 2010). For each photophysiological parameter and each environmental category we concluded from visual evaluation that the relationships are linear and calculated the coefficient of determination (R^2) and the corresponding significance level (p). The results were visualized using raster maps of the coefficient of determination in increments of 0.1 and a complementary map of the p value divided across the critical thresholds 0.050, 0.010 and 0.001. The optimum spectral index representing fluorescence yield is identified based on the highest R^2 between the *in-situ* hyperspectral and fluorescence measurements. This index is regarded as a global index which would sufficiently represent fluorescence yield, and hence photosynthetic activity, based on narrowband spectral channels.

In the context of evaluating our results, we derived 18 narrowband empirical indices reported in the literature. We compared the performance of the empirical indices with the ones we proposed from our own hyperspectral analysis by comparing the R^2 values.

An application of the index proposed on an airborne collected image was finally attempted in order to investigate the different spatial scale of application and the possibility to retrieve information on photosynthesis from remotely sensed data. We identified the indices proposed from the field analyses that can be applicable to airborne imagery. For this reason we applied a 3×3 average filter on the reflectance bands from the field spectra in order to convert them to the spectral resolution of the airborne image. We recomputed the results and located the bands with optimal R^2 values. However, the choice of the optimal index for transferring the methodology to the airborne data depends on the nature of the latter; wavebands at the marginal spectral range of the instrument are dismissed since the instrument noise and the water absorption from the atmosphere above 900 nm result in high levels of errors even after atmospheric correction. Additionally, many of the indices calculated from the raw data lie in a very small part of the spectrum, usually within one or a couple of pixels, and wouldn't be adequate for the spectral resolution of the airborne image. Furthermore, indices based on adjacent bands were tested and provided unsatisfactory results, which can be attributed to the high signal correlation recorded from the instrument. We selected the optimal index for F_s and F_m' based on the above criteria and searched for 2 wavelengths with a sufficient difference in the wavelength of more than 20 nm, a wide waveband more than 10 nm and located outside the regions 300–4000 and 900–1000 nm. We then used the reflectance RSI with the

highest R^2 for F_s and F_m' from the terrestrial part of the transect to plot the $Y(II)$ values calculated from the F_s and F_m' indices according to Eq. (1) against the *in-situ* recorded measurements. RMSE and the R^2 of the linear regression were taken into account to compare the behaviour of the calculated values and the estimated regression from the RSI index. The best bands identified were isolated and the RSI index with the highest statistical significance was applied to the airborne hyperspectral images. The same procedure was carried out for the ETR parameter based on Eq. (2) and by using the result from the $Y(II)$ calculations as above and the best RSI for PAR. The leaf scale reflectance profiles were used as a representation of reed stability on the measurable leaf chemical and physiological properties. The main aspect of this application was to investigate whether the methodology developed at the leaf level could be transferred to airborne imagery and to what extent the result is representative of the real $Y(II)$ and ETR values. For this task and since no accurate fieldwork at canopy level could present the values of $Y(II)$ and ETR, the results were visually interpreted by wetland ecologists at the Balaton Limnological Institute in Tihany to evaluate the information content in the vegetation index image. The performance of the index in regard to reed condition in the study area is further assessed and discussed.

3. Results and discussion

3.1. Spectral and photochemical response of reed leaves in regard to the inundated environment

The spectral reflectance profiles of *Phragmites* leaves measured from the transect of terrestrial, shallow, deep water and waterfront sample locations (Fig. 1) are presented in Fig. 2. We performed a t -test for the bands at 500 nm and 800 nm which represent the optical and near-infrared domains. For the terrestrial and deep water datasets the p value was $1.636e-10$ and $2.2e-16$ respectively for the two wavelengths. Similar results were found for all the four datasets indicating that the discrepancies between categories are statistically important. The leaf reflectance curves of plants growing in terrestrial and shallow water conditions only show very small differences in the visible (<1%) and red-edge (<3%) domains of the spectrum. Their 95% confidence intervals partially overlap, which indicates that they cannot be distinguished based on the visible part but only in the infrared part of the spectrum. The reflectance curves from the deep water and the water's edge locations show differences of up to 5% in the visible and even >10% in the infrared domain when compared to the terrestrial and shallow locations. The vegetation spectra for the deep water and water's edge locations show that their 95% confidence intervals do not overlap with any of the other spectra. They are hence different and responsive to the inundation categories defined. The differences of reflectance profiles found for these levels of inundation can be attributed to the stress condition of the reed patch, the microenvironment in which the culms grow or even differences in genotype of the species growing in different environments (Engloner et al. 2010).

It is important to note that the inundation categories define different ecotypes of the reed bed and hence different reed phenotypic categories. Tóth and Szabó (2012) suggest that morphology of *Phragmites* is influenced by site-specific environmental conditions rather than lake-scale factors. Some of these conditions are increased anaerobic bacterioplankton due to litter accumulation in the reed stands, lack of oxygen in the sediment, anaerobic conditions in the sediment of stagnant waters, reed clones adapted to survive at deep water (lower redox). As a result from these local processes in the succession from the terrestrial to the deep water parts of the reed bed, different ecotypes of *Phragmites* can emerge. Hence the phenotypic variation in such an ecotone can be large, which is prominent in the spectral responses of the categories in our experiment.

The photophysiological data show a high degree of similarity (Fig. 3). The ETR mean values changed throughout the transect between

173 and 222 $\mu\text{mol m}^{-2} \text{s}^{-1}$, although a small, but significant difference in the terrestrial part of the transect was observed. The chlorophyll content of the leaves was ca. 45 SPAD units, with a difference between the deep water and waterfront regions. While on the basis of morphological parameters a special supra-individual ordinance was observed in the transects of the Kerekedi Bay (Tóth & Szabó, 2012) and other experimental setups (Mauchamp et al., 2001; Vretare et al. 2001), the different levels of inundation do not affect the studied photochemical parameters, or this was concealed by the variability within the samples. The relatively high values of the Y(II) and ETR in comparison to earlier studies (Dulai et al., 2002; Mauchamp & Méthy, 2004; Nguyen et al., 2013; Velikova & Loreto, 2005) indicated that the studied plants were in stable condition. The water depth gradient did not affect these studied parameters, although the highest values of ETR and Y(II) were measured in the shallow and deep water part of the reed stand suggesting better conditions for *Phragmites* in these parts of the transect (Fig. 3).

3.2. Complete-combination indices for spectral assessment of photophysiological parameters

Figs. 4 and 5 present an indicative subset of the results of the RSI relationship with Fs and Fm' respectively. Graphs of RSI and NDSI correlations are an information source of significance of the wavelengths correlating to the physiological parameter under study and optimizing the selection of the effective wavelength and bandwidth according to Inoue et al. (2008). With the increasing use of imaging spectroscopy, the need for standardized data processing techniques specifically for hyperspectral data is important (Plaza et al., 2009). These case-specific optimization graphs provide ad-hoc information for the entire hyperspectrum. They are a prime example for analyzing the special properties of hyperspectral data and can be recommended as a process coupling ground data and hyperspectral information. Table 2 summarizes the maximum R^2 and corresponding p values for all the combinations carried out in the experiment. The maximum R^2 values indicate a high correlation and thus a significant predictive ability when using the specific index as a proxy for the physiological parameter. Furthermore, the maps provide information on the effective wavelength bandwidth. For instance, bands with narrow width are appropriate only for hyperspectral data, while bands covering a wider spectrum match the specifications of multispectral instruments.

Reflectance maximum values exhibit differently in regard to individual photophysiological parameters. Fs and Fm' correlation is very similar, which can be attributed to the fact that both Fs and Fm' represent

yield which is proportional to intensity of electromagnetic radiation and thus are directly related to the spectroradiometers' recorded values at specific wavelengths. On the other hand Y(II) and ETR are calculated on the basis of the former. The correlation coefficient in this pair of parameters seems to be close in most cases (Table 2). However, when measuring Y(II) and ETR the reflectance values diverge. Radiance values correlate better in the deep water for Fs and Fm' while Y(II), PAR, ETR and CHL present maximum R^2 at the waterfront part of the transect.

It is important to note the relatively low R^2 obtained for the combined dataset from the whole transect. This indicates that the environmental conditions at the given point of the transect affect essentially the spectral response of *Phragmites* and the inundation categories defined mark important differences between reed stands within a reed bed.

Y(II) is representing the amount of used PSII systems, while ETR shows the actual activity at the given light intensity. Although ETR calculation is based on Y(II), we found that ETR and Y(II) appear to have different effective spectral regions. ETR performs slightly better than Y(II) in terms of maximum R^2 . ETR has the highest correlation $R^2 = 0.65$ at a narrow bandwidth of 3 nm at (493, 478) for both RSI and NDSI at the waterfront category and a sufficient correlation window ($<0.5 R^2 < 0.6$) at 600–700 nm. This bandwidth is typical in multispectral sensors and information can be derived from a combination of bands within this spectral region, which several multispectral sensors contain. Hence, critical information for the ETR parameter is encountered at the red domain of the chlorophyll absorption region. Y(II) has a maximum $R^2 = 0.62$ at (473, 483) for RSI and NDSI.

Comparing the maximum values of R^2 for RSI and NDSI we did not find important differences, however the wavelength combination as well as the shape of the spectral regions in the respective figures changed in several cases. For example, the RSI and NDSI for Fs in the deepwater category are presented in Fig. 7. Both indices sustain similar highest R^2 value (0.76 and 0.75 respectively) at the same combination of wavelengths (633, 690) which is deemed to be significant, despite the very narrow width. Concerning wider wavebands, both indices seem to correlate in a homogeneous spectral area at the wavelengths 530–670 nm and a second region at 690–720 nm in which RSI correlates stronger ($0.6 < R^2 < 0.7$) around 700 nm. In the rest of the results in regard to the category and the photophysiological parameter under study, minor differences can be located in the distribution of the RSI and NDSI maps, however they are insignificant. A comparison of the maximum of the combinations from Table 2 supports the very similar

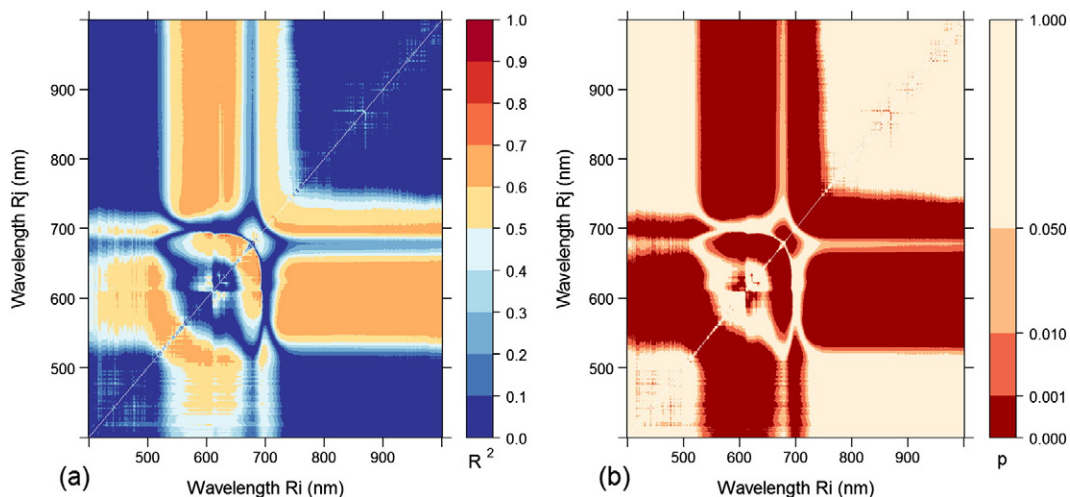


Fig. 4. Coefficient of determination (R^2) (a) and corresponding p values (b) between apparent fluorescence yield (Fs) and RSI (R_i , R_j) measured on *Phragmites australis* plants at the deep water part of the transect in Kerekedi Bay, Lake Balaton. The RSI was calculated using the whole spectrum reflectance combinations of two wavebands at i and j.

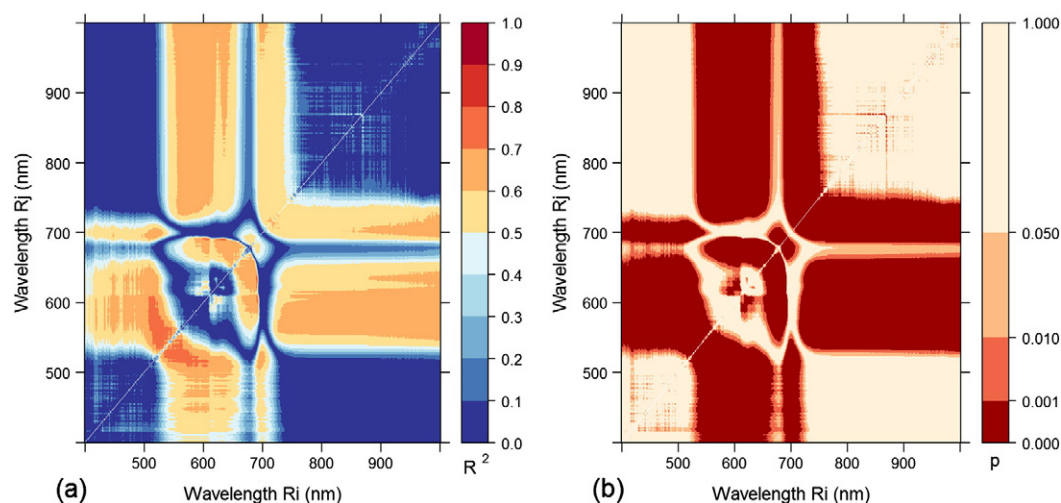


Fig. 5. Coefficient of determination (R^2) (a) and corresponding p values (b) between maximum fluorescence yield (Fm') and RSI (R_i, R_j) measured on *Phragmites australis* plants at the deep water part of the transect in Kerekedi Bay, Lake Balaton. The RSI was calculated using the whole spectrum reflectance combinations of two wavebands at i and j.

maximum R^2 values and wavelength combinations obtained when using the two indices.

3.3. Empirical indices for spectral assessment of photophysiological parameters

18 frequently used empirical indices derived from our *in-situ* spectral measurements according to the 4 inundation categories are presented in Table 3. It is obvious that the best correlations ($R^2 = 0.71$) were obtained from the basic photophysiological parameters (F_s and Fm'), while the derived parameters (i.e. ETR and $Y(II)$) decrease the number of significant correlations found. For F_s and Fm' the highest and more frequent correlation was obtained in the deep water part of the transect, while the waterfront of the studied transect had smaller and less frequent correlations. The latter results could be explained by high homogeneity of the deep water reed stand and the heterogeneity of the studied *Phragmites* in the terrestrial (sporadic appearance of the co-dominant *Carex* and other ruderal species) and waterfront (plants of different ages and physical conditions) parts of the stand. The Photochemical Reflectance Index (PRI) = $(R_{531} - R_{570}) / (R_{531} + R_{570})$

Gamon et al. (1997) has outperformed the other indices and reached R^2 values equal to 0.65 and 0.71 for F_s and Fm' respectively at the deep water category.

Contrary to F_s and Fm' results, for ETR and $Y(II)$ high coefficient correlations are observed in the waterfront category ($R^2 = 0.57^{***}$ and 0.36^* respectively) and are represented better by the narrowband NDVI. We assume that reed standing at the edge of the reed bed is under higher pressure relative to the inner part of the reed bed, therefore diverse physiological states can be encountered and linear correlation with indices representing photosynthetic activity can be optimized.

A comparison of R^2 values between the optimized indices we derived from the complete combinations (Table 2) and the empirical indices (Table 3), reveals that the R^2 values of the proposed narrowband indices are significantly higher than the best performed empirical indices. For instance, regarding F_s in the deep water category, the RSI and NDSI band combinations (690,633) result in $R^2 = 0.76^{***}$ for RSI and $R^2 = 0.75^{***}$ for NDSI while the best empirical index PRI gives 0.65^{***} . For Fm' in the same category, the combination (544, 548) gives $R^2 = 0.82^{***}$ for RSI and NDSI while $PRI = 0.71^{***}$. In the waterfront category, $R^2 = 0.62^{***}$ for $Y(II)$ when calculated from RSI and NDSI while from

Table 1
Empirical indices proposed frequently in remote sensing of vegetation.

Index	Reference	Formula
ARI2 (Anthocyanin Reflectance Index)	Gitelson et al. (2001)	$R_{800} * \left(\frac{1}{R_{530}} - \frac{1}{R_{700}} \right)$
CRI1 (Carotenoid Reflectance Index)	Gitelson et al. (2002)	$\frac{1}{R_{510}} - \frac{1}{R_{550}}$
CRI2 (Carotenoid Reflectance Index)	Gitelson et al. (2002)	$\frac{1}{R_{510}} - \frac{1}{R_{700}}$
EVI (Enhanced Vegetation Index)	Huete et al. (2002)	$2.5 * \frac{R_{750} - R_{675}}{R_{750} + 6 * R_{675} - 7.5 * R_{445} + 1}$
mND ₇₀₅ (modified Normalised Difference Index)	Sims and Gamon (2002)	$\frac{R_{750} - R_{705}}{R_{750} + R_{705} - 2 * R_{445}}$
mSR ₇₀₅ (modified Simple Ratio Index)	Sims and Gamon (2002)	$\frac{R_{750} - R_{445}}{R_{705} - R_{445}}$
NDVI (Normalised Difference Vegetation Index)	Tucker (1979)	$\frac{R_{750} - R_{675}}{R_{750} + R_{675}}$
NDVI ₇₅₀ (Red Edge Normalised Difference Vegetation Index)	Gitelson and Merzlyak (1994)	$\frac{R_{750} - R_{705}}{R_{750} + R_{705}}$
PRI (Photochemical Reflectance Index)	Gamon et al. (1997)	$\frac{R_{531} - R_{570}}{R_{531} + R_{570}}$
PSRI (Plant Senescence Reflectance Index)	Merzlyak et al. (1999)	$\frac{R_{680} - R_{690}}{R_{750}}$
RGI (Red Green Index)	Zarco-Tejada et al. (2005)	$\frac{R_{680}}{R_{550}}$
SGI (Sum Green Index)	Gamon and Surfus (1999)	Mean (R_{680} to R_{690})
SIPI (Structure Insensitive Pigment Index)	Peñuelas et al. (1995)	$\frac{R_{800} - R_{445}}{R_{800} - R_{680}}$
SRI (Simple Ratio Index)	Jordan (1969)	$\frac{R_{800}}{R_{680}}$
VOG1 (Vogelmann)	Vogelmann et al. (1993)	$\frac{R_{750}}{R_{720}}$
VOG2 (Vogelmann)	Vogelmann et al. (1993)	$\frac{R_{734} - R_{547}}{R_{715} + R_{726}}$
VOG3 (Vogelmann)	Vogelmann et al. (1993)	$\frac{R_{734} - R_{547}}{R_{715} + R_{720}}$
WBI (Water Band Index)	Peñuelas et al. (1993)	$\frac{R_{900}}{R_{670}}$

Table 2

Spectral band combination and maximum value of coefficient of determination (R^2) for reflectance RSI and NDSI in regard to the photophysiological parameter measured *in-situ*.
 p: * $\rightarrow p < 0.05$, ** $\rightarrow p < 0.01$, *** $\rightarrow p < 0.001$.

	Terrestrial		Shallow water		Deep water		Waterfront		Combined dataset	
	R_i, R_j	R^2	R_i, R_j	R^2	R_i, R_j	R^2	R_i, R_j	R^2	R_i, R_j	R^2
$RSI = R_i / R_j$										
Fs	541, 549	0.67***	546, 551	0.58***	690, 633	0.76***	871, 861	0.60***	546, 551	0.47***
Fm'	544, 549	0.55***	539, 544	0.57***	545, 548	0.82***	904, 906	0.56***	539, 560	0.47***
Y(II)	803, 818	0.46***	663, 686	0.38***	908, 923	0.45***	473, 483	0.62***	659, 687	0.24***
PAR	945, 941	0.48***	892, 889	0.25***	827, 825	0.48***	989, 997	0.71***	917, 922	0.09***
ETR	941, 945	0.52***	664, 685	0.47***	556, 564	0.48***	493, 478	0.65***	621, 692	0.25***
CHL	802, 800	0.51***	759, 764	0.57***	760, 764	0.50***	889, 924	0.63***	747, 748	0.14***
$NDSI = (R_i - R_j) / (R_i + R_j)$										
Fs	541, 549	0.67***	546, 551	0.58***	633, 690	0.75***	861, 871	0.60***	546, 551	0.47***
Fm'	544, 549	0.55***	539, 544	0.57***	545, 548	0.82***	904, 906	0.56***	539, 560	0.47***
Y(II)	803, 818	0.46***	663, 686	0.38***	908, 923	0.45***	473, 483	0.62***	659, 687	0.24***
PAR	941, 945	0.48***	889, 892	0.25***	825, 827	0.48***	989, 997	0.71***	917, 922	0.09***
ETR	941, 945	0.52***	664, 685	0.47***	556, 564	0.48***	478, 493	0.65***	621, 692	0.25***
CHL	800, 802	0.51***	759, 764	0.57***	760, 764	0.50***	889, 924	0.63***	747, 748	0.14***

$NDVI R^2 = 0.36^{***}$. In a similar manner and for ETR, $R^2 = 0.65^{***}$ for RSI and NDSI while for NDVI $R^2 = 0.57^{***}$. The results are in some way anticipated, at least concerning PRI and NDVI; these two empirical indices are each a specific case of NDSI and the result from their calculation has been already accounted for in the complete combination bands. Comparing the PRI band combination (531, 570) with the optimized one for Fs in the terrestrial part (541, 549), it is noticeable that these two indices lay in the same 2-dimensional spectral region, and hence the results are expected to be similar. By testing the complete combination bands we identified the exact bands which provide optimum coefficient correlation for a specific case study. This becomes obvious in Fig. 6 where we visualize the relationship between all spectral indices in the form of correlation clusters for the shallow water part category. Nevertheless, mathematically more complicated empirical indices such as EVI didn't perform satisfactorily. This fact in combination with the observation that RSI and NDSI are very similar in our results as well as in results of similar studies (e.g. Inoue et al., 2012) can lead to the conclusion that the importance

of constructing a spectral index lies in the band selection and not the mathematical formulae.

3.4. Estimation of Y(II) and ETR from RSI values

3.4.1. Y(II) estimation

For the maximum values of the correlations found between the photophysiological parameters Fs and Fm' and the corresponding RSIs, the linear regression was calculated on the dataset collected at the terrestrial part of the transect according to Eq. (1) (Fig. 8 and Table 4). Based on the values of Fs and Fm' for each measurement, the Y(II) was calculated and the linear regression between the latter modelled Y(II) and the *in-situ* measurement for Y(II) recorded was investigated for each category. The R^2 of the model predictions was for most cases considerably lower than the calculated from the RSI. Only the terrestrial modelling prediction is distinguished by providing a correlation of 0.35 (Fig. 9) while the estimated correlation from the best *in-situ* RSI was 0.46. The corresponding RMSE was found to be 0.057.

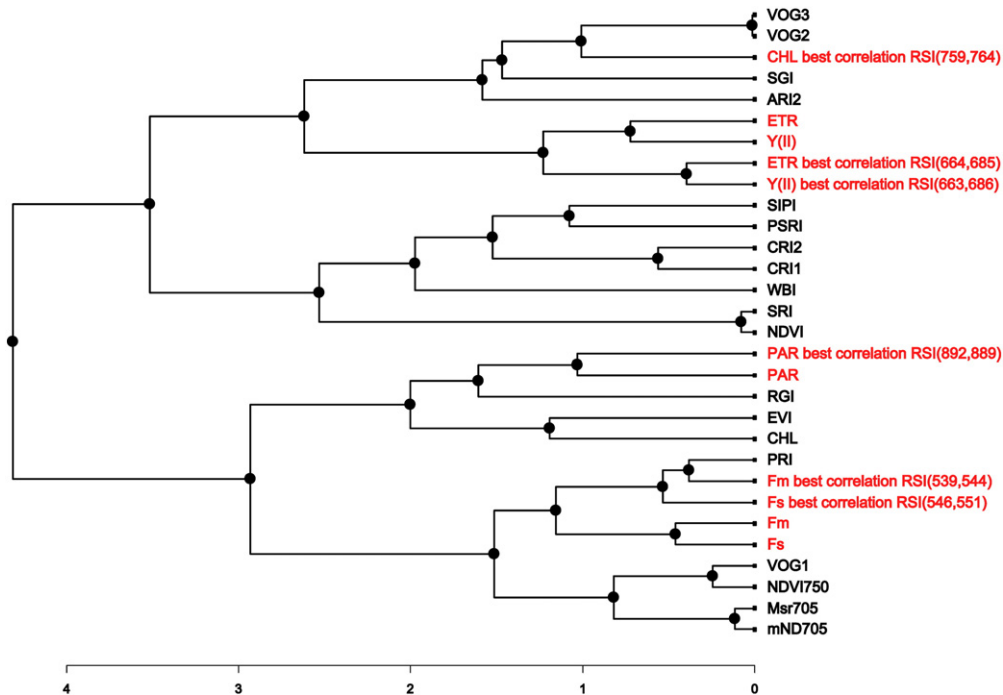


Fig. 6. Hierarchical clustering of correlation relationship between the spectral indices proposed, the empirical indices tested and the biophysical parameters measured *in-situ*.

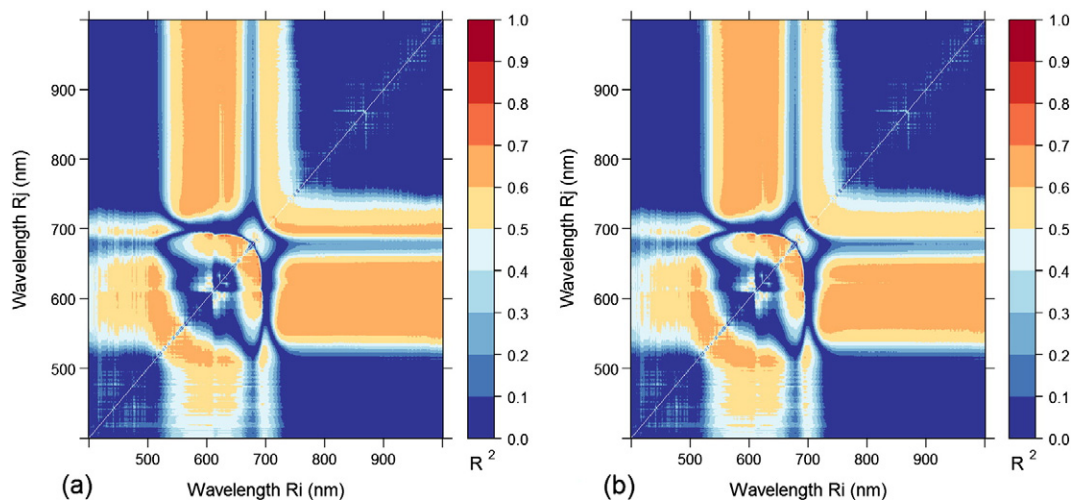


Fig. 7. Coefficient of determination (R^2) for RSI (R_i, R_j) (a) and NDSI (R_i, R_j) (b) between F_s measured on *Phragmites australis* plants at the deepwater part of the transect in Kerekedi Bay, Lake Balaton. RSI and NDSI were calculated using the whole reflectance spectrum combinations of two wavebands at i and j .

3.4.2. ETR estimation

In a similar manner we calculated the ETR for the reed on the water-front part of the transect on the basis of the maximum RSI values for PAR and Y(II) (Fig. 10). The predicted R^2 value was found to be 0.72 (Fig. 11)

while the R^2 value from the *in-situ* ETR correlation with the best RSI was 0.65. This indicated that the modelled prediction based on Eq. (2) provides a slightly higher R^2 values for ETR. The corresponding RMSE was 49.707. The results for the other parts of the transect (Table 5) indicate

Table 3
Correlation matrix between the measured photophysiological parameters and empirical indices. *: $p < 0.05$, **: $p < 0.01$, ***: $p < 0.001$, all the numbers without significance indexes are not significant.

	F_s	F_m'	Y(II)	PAR	ETR	CHL	F_s	F_m'	Y(II)	PAR	ETR	CHL
Terrestrial						Shallow water						
ARI2	0.3**	0.33**	0.01	0.03	0.02	0.22*	0.18**	0.24***	0.04	0	0.07	0.03
CRI1	0.07	0.06	0.03	0.02	0.12	0.25*	0.1*	0.06	0.13**	0.03	0.09*	0.01
CRI2	0.12	0.11	0.03	0.01	0.09	0.29**	0.14**	0.11*	0.14**	0.02	0.11*	0.01
EVI	0.4**	0.32**	0.08	0.03	0	0.02	0.01	0.02	0	0.01	0.01	0.23***
mND ₇₀₅	0.25*	0.31**	0	0.02	0.02	0.23*	0.15**	0.21***	0.02	0	0.02	0.23***
mSR ₇₀₅	0.26*	0.3**	0.01	0.01	0.02	0.23*	0.16**	0.21***	0.02	0	0.03	0.19***
NDVI	0	0	0	0.05	0.12	0.15	0.04	0.07*	0	0.03	0.01	0
NDVI ₇₅₀	0.22*	0.28**	0	0.01	0.01	0.1	0.18**	0.26***	0.01	0	0.02	0.24***
PRI	0.62***	0.45***	0.22*	0	0.17	0.03	0.48***	0.52***	0.22***	0	0.26***	0
PSRI	0	0.01	0.04	0.15	0.07	0.01	0.04	0.03	0.07	0	0.08*	0.03
RGI	0.01	0.03	0	0.15	0.17	0.18*	0	0	0	0.03	0.01	0.2***
SGI	0.08	0.06	0.01	0	0	0.01	0.08*	0.14**	0	0.01	0.01	0.06
SIPI	0	0	0.04	0.17*	0.1	0.08	0	0	0	0	0	0
SRI	0	0	0.01	0.05	0.14	0.15	0.03	0.07	0	0.04	0.01	0.01
VOG1	0.18*	0.25*	0	0.02	0.01	0.14	0.17**	0.24***	0.02	0	0.02	0.31***
VOG2	0.14	0.21*	0	0.02	0	0.16	0.15**	0.22***	0.01	0	0.01	0.35***
VOG3	0.14	0.22*	0	0.02	0	0.16	0.15**	0.22***	0.01	0	0.01	0.35***
WBI	0.13	0.07	0.05	0	0.01	0.01	0	0	0	0	0	0
Deep water						Waterfront						
ARI2	0.39***	0.4***	0.08	0.01	0.14	0.13	0.02	0	0.03	0.06	0.09	0.31*
CRI1	0.38***	0.46***	0.04	0.01	0.09	0.15*	0.07	0.03	0.14	0.15	0.24*	0.28*
CRI2	0.43***	0.5***	0.05	0.01	0.11	0.16*	0.05	0.03	0.1	0.1	0.17	0.36*
EVI	0.01	0.07	0.05	0.04	0.01	0.1	0.05	0	0.26*	0.19	0.41**	0.42**
mND ₇₀₅	0.57***	0.61***	0.1	0	0.1	0.14	0.01	0	0.11	0.34*	0.35*	0.01
mSR ₇₀₅	0.65***	0.63***	0.17*	0	0.17*	0.1	0.01	0	0.08	0.26*	0.27*	0.01
NDVI	0.21*	0.16*	0.16*	0.01	0.12	0	0.17	0.04	0.36*	0.31*	0.57***	0.1
NDVI ₇₅₀	0.56***	0.58***	0.13	0	0.11	0.17*	0.04	0	0.22	0.38**	0.5**	0.04
PRI	0.65***	0.71***	0.14	0.04	0.27**	0.02	0.05	0.06	0.03	0.03	0	0.33*
PSRI	0.08	0.14	0	0.2*	0.1	0.01	0	0	0.02	0.04	0.04	0.4**
RGI	0.09	0.12	0	0.04	0.02	0.21*	0.19	0.11	0.17	0.03	0.18	0.01
SGI	0.28**	0.27**	0.08	0	0.09	0	0.01	0	0.07	0.37**	0.31*	0.13
SIPI	0.1	0.13	0.01	0.04	0.05	0.03	0	0.01	0.02	0.02	0.02	0.44**
SRI	0.21*	0.16*	0.16*	0.01	0.12	0	0.12	0.03	0.3*	0.27*	0.5**	0.13
VOG1	0.56***	0.58***	0.12	0.01	0.1	0.21*	0.02	0	0.21	0.36*	0.47**	0.05
VOG2	0.55***	0.56***	0.12	0.01	0.09	0.23*	0.01	0.01	0.2	0.32*	0.44**	0.06
VOG3	0.55***	0.57***	0.13	0.01	0.09	0.23*	0.01	0.01	0.2	0.32*	0.43**	0.06
WBI	0.04	0.02	0.04	0.03	0.01	0.14	0.01	0.06	0.05	0.02	0.06	0.2

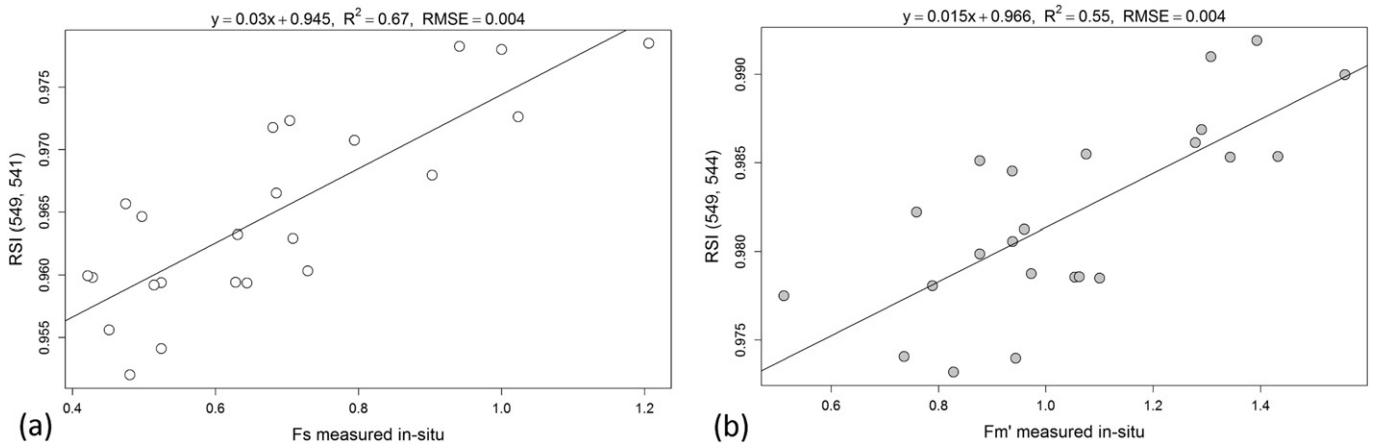


Fig. 8. Linear regression for Fs (a) and Fm' (b) for the reflectance RSIs with the highest correlations at the terrestrial part of the transect in Kerekedi Bay, Lake Balaton.

that the predicted R^2 value is always lower than the measured, however the differences are not significant. In comparison to the prediction of Y(II), prediction of ETR seems to perform better in terms of the coefficient of determination values.

The experimental design introduces some unavoidable limitations in correlation and therefore generally cannot lead to exceptionally high R^2 values. The paired dataset is acquired from two different scientific electronic instruments with different setups, operations and associated errors. Furthermore, while measurements were made on the same area of each leaf, the overlap due to the users' operation accuracy is not certain, as well as the effective surface is not identical in the two instruments and neither could be compensated. An additional source of variability is reed vegetation location, as it lies in a land–water ecotone and is ecologically highly variable while the use of categories adapted assumes crisp boundaries. Finally Y(II) is a measurement of the efficiency of PSII photochemistry and ETR a proxy of the gross rate of carbon fixation, the latter is assumed to represent photosynthesis (Maxwell & Johnson, 2000). A high correlation is found under laboratory conditions between these relationships, however when measured in the field, Y(II) and CO_2 fluxes can be affected by temperature (Fryer et al. 1998). All the above errors are introduced and propagate throughout the experiment, thus the correlation coefficient estimated is not as high as in similar studies investigating direct morphological and physiological aspects (i.e. stem density, dry biomass, chlorophyll and nitrogen content with laboratory methods), nevertheless coupling with fluorescence data provides a direct representation of photosynthetic activity of the plant.

3.5. Application on airborne hyperspectral data

When the findings from the leaf scale are used for interpretation of airborne imagery, some confounding factors need first to be considered. Airborne reflectance measurements are made at a coarser scale and tend to average over a very large number of leaves, which may include healthy and diseased leaves, stems or even leaves from different species. Furthermore, shadows caused by the vegetation and orientation of the

leaves are largely affecting the illumination conditions of canopy reflectance. In addition, in sparse vegetative conditions understory vegetation, ground or water signal can add in to the radiant exitance within a pixel. This is a limitation of a direct application of the findings from the field spectroradiometry to canopy level airborne imagery.

The optimal index for the application on the airborne dataset was defined as the band combination with the highest R^2 value from the filtered 3×3 results, a corresponding confident p value, the lowest RMSE and also covers a sufficiently broad spectrum to contain the remote sensors bandwidth at the specific wavelength. This has been identified as the band combinations RSI(612, 516) (0.63***) for Fs, (699, 527) (0.51***) for Fm' and (463, 488) (0.47***) for PAR based on the terrestrial category. The Y(II) and ETR maps resulting from transferring the field methodology to the airborne imagery are presented in Fig. 11. The Y(II) calculated on the basis of Fs and Fm' parameters reveals the photophysiological homogeneity over the stable reed and is sufficient for estimation of the Y(II) value based on remotely sensed data. This becomes obvious by comparing the map with the actual Y(II) measurements *in-situ* (Fig. 3). The terrestrial and waterfront sides of the stand have slightly lower Y(II) values, while the reed stands in the middle of the reed bed contain higher values (Figs. 3 and 12). The calculated Y(II) values are lower by 15–20% compared to the *in-situ* actual data, but insertion of a correction factor could compensate for the final output. In spatially more heterogeneous environments, such as the waterfront and terrestrial edges, the potential photosynthetic capacity is lower than in the more homogeneous environment in the middle of the reed bed. This is probably in connection with disturbances that the plant is encountering at less homogeneous patches. Moreover in these sites the possibility of appearance of adventive species is significantly higher, thus different ETR and Y(II) signals could be originated from the abundance of other species within a single pixel. Furthermore, the waterfront of the reed stands contains plants of significant age differences (Tóth & Szabó, 2012) which affects the photophysiological parameters too, while the interior of the stands has a more homogeneous age distribution and thus more reliably measured by remote sensing. Thus,

Table 4
Model predictions for Y(II) from the RSI reflectance dataset.

	Equation	RMSE	R^2 from predicted Y(II)	R^2 from best RSI for Y(II) – Table 1
Terrestrial	$y = 0.443x + 0.231$	0.057	0.35 (Fig. 9)	0.46
Shallow water	$y = 0.873x + 0.074$	0.167	0.12	0.38
Deep water	$y = 0.456x + 0.236$	0.131	0.05	0.45
Waterfront	$y = 1.395x - 0.200$	0.180	0.27	0.62
Combined dataset	$y = 0.513x + 0.180$	0.334	0.01	0.24

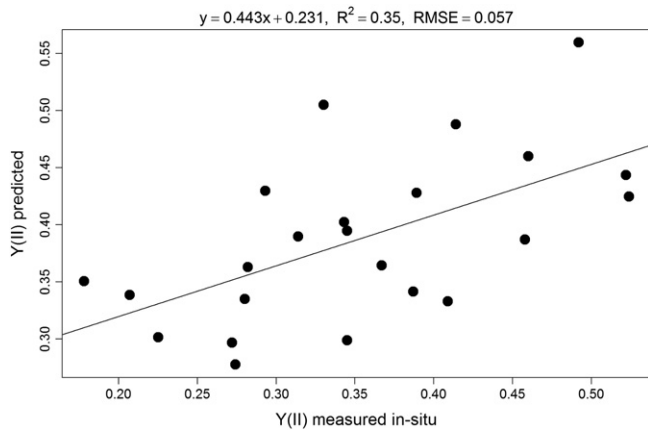


Fig. 9. Linear regression of the measured and predicted values for Y(II) of *Phragmites* plants from the terrestrial part of the transect. Predicted values calculated based on the best correlations found from reflectance RSI for Fs and Fm' (Fig. 8).

while during the *in-situ* fluorescence measurements the average and fully grown plants were usually measured, the airborne data contains the spectral response from a very diverse pool of *Phragmites* plants including the very strong signal from young shoots. It is worth noting here that spectra of similar materials are recorded differently from the ASD and the Eagle sensors due to the fact that airborne remote-sensing systems measure the amount of radiation reflected by an object which varies depending upon the sensitivity of the instrument, the wavelengths sampled, lighting geometry and atmospheric conditions (Roberts & Herold, 2004) rather than reflectance. Moreover, there is a 2-year time difference between the field and airborne measurements contributing to the variation. Another source of variation is the Bidirectional Reflectance Distribution Function (BRDF) affecting the airborne data. Although a compensation for that has not been attempted in the lack of multi-directional data, this might have introduced variations in the illumination of the area. Additionally, the spectral resolution of the airborne instrument was set to maximum (i.e. <3 nm) during the acquisition of the data, which resulted to suboptimal signal-to-noise ratio. Consequently, the marginal spectral regions will be noisy and the indices proposed from the field analysis that lie in these areas will not be applicable. Especially in regard to estimating biophysical parameters in optically complex waters, errors associated only to SNR can account as high as 80% for space borne hyperspectral sensors as demonstrated by Moses et al. (2012). Furthermore, low radiometric resolution means high correlation between adjacent channels, and application of indices to the

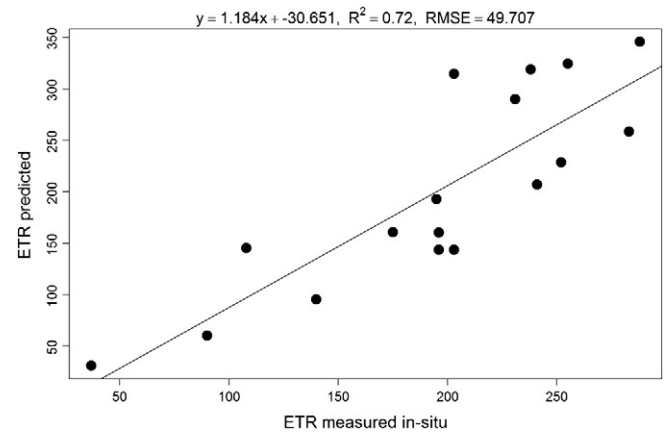


Fig. 11. Linear regression of the measured and predicted values for ETR of *Phragmites* plants from the waterfront part of the transect. Predicted values calculated based on the best correlations found from reflectance RSI for PAR and Y(II) (Fig. 10).

airborne data based on these channels will provide a noisy output. Hence the selection of the Fs and Fm' was based on the highest correlation among the indices which are not encountered in the regions 400–450 nm and 900–1000 nm and they have a sufficient spectral difference of 10 nm.

The map derived from direct correlation between the spectral data and fluorescence base data (Fs and Fm') and later calculated into Y(II) and ETR (Fig. 12) presents an anticipated distribution of reed physiological status in Kerekedi Bay. Although the photophysiological measurements did not show spatial differentiation, the airborne derived Y(II) and ETR data showed significant, site specific differences (Fig. 12). These differences mostly correlated with the measured data (Fig. 3c and d), except that the highest parameters (and thus the reed predicted as most stable) were observed in the waterfront of the studied *Phragmites* stand. This significant difference between the measured photophysiological parameters and derived Y(II) and ETR could be explained by methodological differences.

In summary, we propose that the photosynthetic activity can be estimated from hyperspectral airborne imagery. The images have to be radiometrically and atmospherically corrected in order to assure consistency between the remotely sensed data and leaf data. This methodology has been successfully demonstrated when applied to high spectral and spatial resolution airborne imagery. Based on the reflectance spectral indices (612, 516) (0.63***) for Fs, (699, 527) (0.51***) for Fm' and (463, 488) (0.47***) and Eqs. (1) and (2) estimation of Y(II) and ETR is

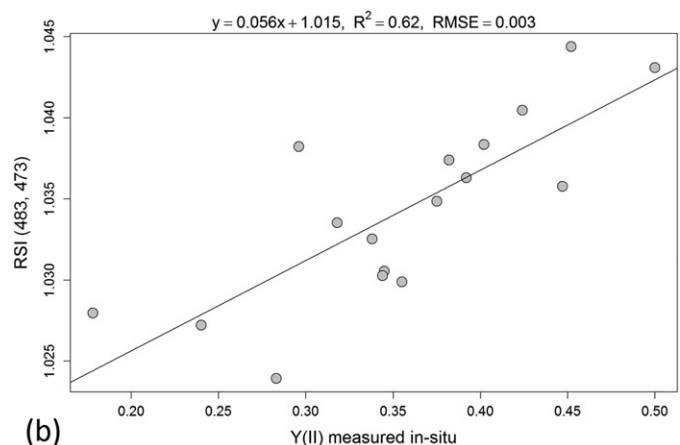
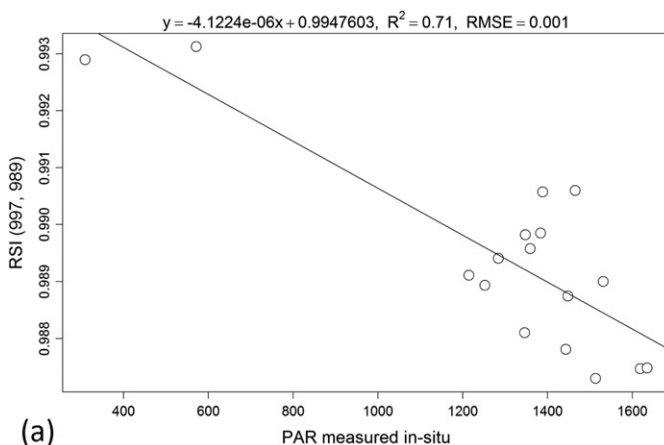


Fig. 10. Linear regression for PAR (a) and Y(II) (b) for the reflectance RSIs with the highest correlations at the waterfront part of the transect in Kerekedi Bay, Lake Balaton.

Table 5

Model predictions for ETR from the RSI reflectance dataset.

	Equation	RMSE	R ² from predicted ETR	R ² from best RSI for ETR – Table 1
Terrestrial	$y = 1.098x - 55.703$	66.329	0.48	0.52
Shallow water	$y = 1.247x - 43.055$	58.587	0.38	0.47
Deep water	$y = 1.024x + 12.544$	52.96	0.37	0.48
Waterfront	$y = 1.184x - 30.651$	49.707	0.72 (Fig. 11)	0.65
Combined dataset	$y = 1.247x - 37.723$	134.89	0.17	0.25

feasible qualitatively. When applying a linear regression to fit the spectral indices to the *in-situ* observations according to the equations in Table 4, quantitative estimation of Y(II) and ETR is possible. While the study area comprised mainly of stable reed, reed areas receiving environmental pressure appear at marginal values. This methodology could be used to map the physiological status of reed beds based solely on hyperspectral imagery.

4. Conclusion

Spectroradiometric leaf reflectance and photophysiological parameters were measured *in-situ* over reed leaves in different inundation categories at vegetation peak in a mesotrophic basin of Lake Balaton, Hungary. No effect of inundation on photophysiological parameters across different water levels along a transect vertical to the lake shore was found, however the spectral response diversifies significantly. A strong correlation between narrowband spectral indices and chlorophyll fluorescence parameters indicates the potential of *in-situ* hyperspectral data in assessing plant stability. We found that for *in-situ* hyperspectral leaf measurements, the index (690, 633) provides the best coefficient correlation (0.76***) for Fs in the stable deep water part of the transect and (545, 548) (0.82***) for the Fm'. In the waterfront category, Y(II) correlates better with the band combination (473, 483) (0.62***) and ETR with (493, 478) (0.65***). While these indices are spectrally very narrow and can be applied only when the instrument has a very high spectral resolution of 1 nm, maps of the coefficient of determination can aid locating indices tailored to other remote sensing instruments. An application of the findings from the field data analysis to the airborne hyperspectral imagery on the study area presents actual estimation of Y(II) and ETR values over the reed bed under study. The indices identified were Fm': (699, 527) and Fs: (612, 516) for calculating Y(II) and PAR: (463, 488) for calculating ETR on the basis of mathematical equations.

This research underpins the development of methods for estimating photophysiological parameters on *Phragmites* based solely on imaging spectroscopy and proposes optimal indices for evaluating reed ecological status based on spectroscopic data. Future work will encompass samples from a reed population comprising of stable and die-back reed, which will provide die-back specific indicators.

Acknowledgements

This research is supported by GIONET, funded by the European Commission, Marie Curie Programme, Initial Training Networks, Grant Agreement number PITN-GA-2010-264509. We wish to acknowledge the Airborne Research and Survey Facility (ARSF, Gloucester, U.K.) vested in the Natural Environment Research Council (NERC) for the collection and provision of the airborne dataset. We also express our gratitude to the three anonymous reviewers for their fruitful remarks.

References

- Baker, N. R. (2008). Chlorophyll fluorescence: A probe of photosynthesis in vivo. *Annu Rev Plant Biol*, 59, 89–113.
- Bresciani, M., Sotgia, C., Fila, L.-G., Musanti, M., & Bolpagni, R. (2011). Assessing common reed bed health and management strategies in Lake Garda (Italy) by means of Leaf Area Index measurements. *Italian Journal of Remote Sensing*, 43(2), 9–22.
- Bresciani, M., Stroppiana, D., Fila, G., Montagna, M., & Giardino, C. (2009). Monitoring reed vegetation in environmentally sensitive areas in Italy. *Italian Journal of Remote Sensing*, 41(2), 125–137.
- Brix, H. (1999). The European research project on reed die-back and progression (EUREED). *Limnologia – Ecology and Management of Inland Waters*, 29(1), 5–10.
- Dulai, S., Horváth, F., Pécsvárdi, A., Bondár, M., Molnár, I., & Erdei, L. (2002). Does increased photorespiration protect the leaves of common reed living in fragmented patches from excess light. *Acta Biologica Szegediensis*, 46(3–4), 155–156.
- Engloner, A. I. (2009). Structure, growth dynamics and biomass of reed (*Phragmites australis*) – A review. *Flora – Morphology, Distribution, Functional Ecology of Plants*, 204(5), 331–346.
- Engloner, A. I., Major, A., & Podani, J. (2010). Clonal diversity along a water depth gradient in a declining reed stand as detected by three different genetic methods. *Aquatic Botany*, 92(1), 1–8.
- Fogli, S., Marchesini, R., & Gerdol, R. (2002). Reed (*Phragmites australis*) decline in a brackish wetland in Italy. *Marine environmental research*, 53(5), 465–479.
- Fryer, M. J., Andrews, J. R., Oxborough, K., Blowers, D. A., & Baker, N. R. (1998). Relationship between CO₂ assimilation, photosynthetic electron transport, and active O₂ metabolism in leaves of maize in the field during periods of low temperature. *Plant Physiol.*, 116, 571–580.
- Gamon, J. A., Serrano, L., & Surfus, J. S. (1997). The photochemical reflectance index: An optical indicator of photosynthetic radiation use efficiency across species, functional types and nutrient levels. *Oecologia*, 112, 492–501.
- Gamon, J. A., & Surfus, J. (1999). Assessing leaf pigment content and activity with a reflectometer. *New Phytologist*, 143(1), 105–117.
- Genty, B., Briantais, J. M., & Baker, N. R. (1989). The relationship between the quantum yield of photosynthetic electron transport and quenching of chlorophyll fluorescence. *Biochimica et Biophysica Acta (BBA) – General Subjects*, 990(1), 87–92.

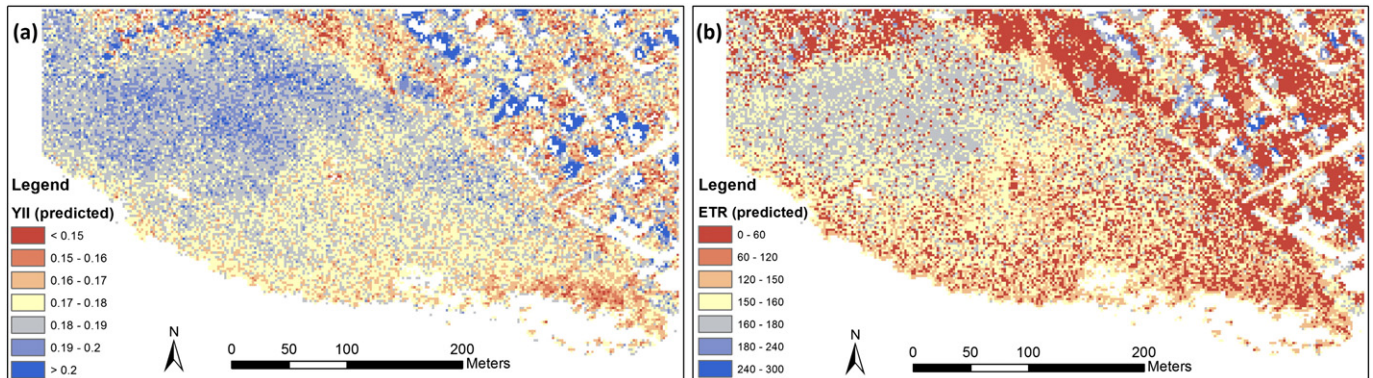


Fig. 12. Y(II) (a) and ETR (b) estimation from the hyperspectral airborne dataset over the area of study at Kerekedi Bay, Lake Balaton according to the best correlation found in the reflectance RSI at the terrestrial part of the transect (left) and predicted values calculated from the maximum correlation of Fs and Fm'.

- Gitelson, A. A., & Merzlyak, M. N. (1994). Spectral reflectance changes associated with autumn senescence of *Aesculus hippocastanum* L. and *Acer platanoides* L. leaves. Spectral features and relation to chlorophyll estimation. *Journal of Plant Physiology*, 143, 286–292.
- Gitelson, A. A., & Merzlyak, M. M. (1996). Signature analysis of leaf reflectance spectra: Algorithm development for remote sensing of chlorophyll. *Journal of Plant Physiology*, 148(3–4), 494–500.
- Gitelson, A. A., Merzlyak, M. N., & Chivkunova, O. B. (2001). Optical properties and non-destructive estimation of anthocyanin content in plant leaves. *Photochemistry and Photobiology*, 71, 38–45.
- Gitelson, A. A., Zur, Y., Chivkunova, O. B., & Merzlyak, M. N. (2002). Assessing carotenoid content in plant leaves with reflectance spectroscopy. *Photochemistry and Photobiology*, 75, 272–281.
- Haslam, S. M. (1969). The development of shoots in *Phragmites communis* Trin. *Annals of Botany*, 33(4), 695–709.
- Huete, A., Didan, K., Miura, T., Rodriguez, E. P., Gao, X., & Ferreira, L. G. (2002). Overview of the radiometric and biophysical performance of the MODIS vegetation indices. *Remote Sensing of Environment*, 83, 195–213.
- Hunter, P. D., Gilvear, D. J., Tyler, A. N., Willby, N. J., & Kelly, A. (2010). Mapping macrophytic vegetation in shallow lakes using the Compact Airborne Spectrographic Imager (CASI). *Aquatic Conservation: Marine and Freshwater Ecosystems*, 20, 717–727.
- Hürlimann, H. (1951). Zur Lebensgeschichte des Schilfs an den Ufern der Schweizer Seen. Switzerland. *Beiträge zur geobotanischen Landesaufnahme der Schweiz*, 30, 1–232 (In German).
- Inoue, Y., Peñuelas, J., Miyata, A., & Mano, M. (2008). Normalized difference spectral indices for estimating photosynthetic efficiency and capacity at a canopy scale derived from hyperspectral and CO₂ flux measurements in rice. *Remote Sensing of Environment*, 112, 156–172.
- Inoue, Y., Sakaiya, E., Zhu, Y., & Takahashi, W. (2012). Diagnostic mapping of canopy nitrogen content in rice based on hyperspectral measurements. *Remote Sensing of Environment*, 126, 210–221.
- Jordan, C. F. (1969). Derivation of leaf area index from quality of light on the forest floor. *Ecology*, 50, 663–666.
- Kovács, M., Turcsányi, G., Tuba, Z., Wolcsanszky, S. E., Vasarhelyi, T., Dely-Draskovits, A., et al. (1989). The decay of reed in Hungarian lakes. *Symposia Biologica Hungarica*, 38, 461–471.
- Krause, G. H., & Weis, E. (1991). Chlorophyll fluorescence and photosynthesis: The basics. *Annual Review of Plant Physiology and Plant Molecular Biology*, 42, 313–349.
- Liira, J., Feldmann, T., Mäemets, H., & Peterson, U. (2010). Two decades of macrophyte expansion on the shores of a large shallow northern temperate lake – A retrospective series of satellite images. *Aquatic Botany*, 93(4), 207–215.
- Mauchamp, A., Blanch, S., Grillas, P., Mauchamp, A., Blanch, S., & Grillas, P. (2001). Effects of submergence on the growth of *Phragmites australis* seedlings. *Aquatic Botany*, 69(2–4), 147–164 (Special issue on *Phragmites*-dominated wetlands, their functions and sustainable use).
- Mauchamp, A., & Méthy, M. (2004). Submergence-induced damage of photosynthetic apparatus in *Phragmites australis*. *Environmental and experimental botany*, 51(3), 227–235.
- Maxwell, K., & Johnson, G. N. (2000). Chlorophyll fluorescence – A practical guide. *Journal of Experimental Botany*, 51, 659–668.
- Merzlyak, M. N., Gitelson, A. A., Chivkunova, O. B., & Rakitin, V. Y. (1999). Non-destructive optical detection of pigment changes during leaf senescence and fruit ripening. *Physiologia Plantarum*, 106(1), 135–141.
- Moses, W. J., Bowles, J. H., Lucke, R. L., & Corson, M. R. (2012). Impact of signal-to-noise ratio in a hyperspectral sensor on the accuracy of biophysical parameter estimation in case II waters. *Optics Express*, 20(4), 4309–4330.
- Nguyen, L. X., Lambertini, C., Sorrell, B. K., Eller, F., Achenbach, L., & Brix, H. (2013). Photosynthesis of co-existing *Phragmites* haplotypes in their non-native range: Are characteristics determined by adaptations derived from their native origin. *AoB Plants*, 5 (pl016).
- Onojeghuo, A. O., & Blackburn, G. A. (2011). Optimising the use of hyperspectral and LiDAR data for mapping reedbed habitats. *Remote Sensing of Environment*, 115(8), 2025–2034.
- Ostendorp, W. (1989). Die-back' of reeds in Europe – A critical review of literature. *Aquatic Botany*, 35(1), 5–26.
- Paillisson, J.-M., & Marion, L. (2011). Water level fluctuations for managing excessive plant biomass in shallow lakes. *Ecological Engineering*, 37(2), 241–247.
- Peñuelas, J., Baret, F., & Filella, I. (1995). Semi-empirical indices to assess carotenoids/chlorophyll *a* ratio from leaf spectral reflectance. *Photosynthetica*, 31(2), 221–230.
- Peñuelas, J., Filella, I., Biel, C., Serrano, L., & Save, R. (1993). The reflectance at the 950–970 nm region as an indicator of plant water status. *International Journal of Remote Sensing*, 14(10), 1887–1905.
- Plaza, A., Benediktsson, J. A., Boardman, J. W., Brazile, J., Bruzzone, L., Camps-Valls, G., et al. (2009). Recent advances in techniques for hyperspectral image processing. *Remote Sensing of Environment, Imaging Spectroscopy Special Issue*, 113(Supplement 1), S110–S122.
- R Core Team (2013). *R: A language and environment for statistical computing*. Vienna, Austria: R Foundation for Statistical Computing.
- Roberts, D. A., & Herold, M. (2004). Imaging spectrometry of urban materials. Available online at: http://www.geogr.uni-jena.de/~cshema/spec/imaging_spectrometry_of_urban_materials.pdf (accessed 29 March 2011)
- Rouse, J. W., Haas, R. H., Schell, J. A., & Deering, D. W. (1974). Monitoring vegetation systems in the Great Plains with ERTS. *Proc. Third ERTS-1 Symposium, NASA Goddard, NASA SP-351* (pp. 309–317).
- Sims, D. A., & Gamon, J. A. (2002). Relationships between leaf pigment content and spectral reflectance across a wide range of species, leaf structures and developmental stages. *Remote Sensing of Environment*, 81(2–3), 337–354.
- Stagakis, S., Markos, N., Sykioti, O., & Kyparissis, A. (2010). Monitoring canopy biophysical and biochemical parameters in ecosystem scale using satellite hyperspectral imagery: An application on a *Phlomis fruticosa* Mediterranean ecosystem using multiangular CHRIS/PROBA observations. *Remote Sensing of Environment*, 114(5), 977–994.
- Thenkabail, P. S., Lyon, J. G., & Huete, A. (2012). Hyperspectral remote sensing of vegetation. XXXV. (pp. 705). CRC Press 9781439845370.
- Thenkabail, P. S., Smith, R. B., & Pauw, E. D. (2000). Hyperspectral vegetation indices and their relationships with agricultural crop characteristics. *Remote Sensing of Environment*, 71, 158–182.
- Tóth, L., Felföldy, L., & Szabó, E. (1961). A Balatoni nádas-termelés méréseinek néhány problémájáról. *Annales Instituti Biologici (Tihany) Hungariae Academiae Scientiarum*, 28, 168–179 (in Hungarian).
- Tóth, V. R., & Szabó, K. (2012). Morphological structural analysis of *Phragmites australis* stands in Lake Balaton. *Ann. Limnol.- Int. J. Lim.*, 48, 241–251.
- Tucker, C. J. (1979). Red and photographic infrared linear combinations for monitoring vegetation. *Remote Sensing of the Environment*, 8, 127–150.
- Tucker, G. C. (1990). The Genera of Arundinoideae (Gramineae) in the Southeastern United States. *Journal of the Arnold Arboretum*, 71(2), 145–177.
- Van der Putten, W. H. (1997). Die-back of *Phragmites australis* in European wetlands: An overview of the European Research Programme on Reed Die-Back and Progression (1993–1994). *Aquatic Botany*, 59(3–4), 263–275.
- Velikova, V., & Loreto, F. (2005). On the relationship between isoprene emission and thermotolerance in *Phragmites australis* leaves exposed to high temperatures and during the recovery from a heat stress. *Plant, Cell & Environment*, 28(3), 318–327.
- Villa, P., Laini, A., Bresciani, M., & Bolpagni, R. (2013). A remote sensing approach to monitor the conservation status of lacustrine *Phragmites australis* beds. *Wetlands Ecology and Management*. <http://dx.doi.org/10.1007/s11273-013-9311-9>.
- Virág, Á. (1997). *A Balaton múltja és jelene*. Eger: Egri Nyomda Rt (In Hungarian).
- Vogelmann, J. E., Rock, B. N., & Moss, D. M. (1993). Red edge spectral measurements from sugar maple leaves. *International Journal of Remote Sensing*, 14(8), 1563–1575.
- Vretare, V., Weisner, S. E. B., Strand, J. A., & Graneli, W. (2001). Phenotypic plasticity in *Phragmites australis* as a functional response to water depth. *Aquatic Botany*, 69, 127–145.
- Zarco-Tejada, P. J., Berjón, A., López-Lozano, R., Miller, J. R., Martín, P., Cachorro, V., et al. (2005). Assessing vineyard condition with hyperspectral indices: Leaf and canopy reflectance simulation in a row-structured discontinuous canopy. *Remote Sensing of Environment*, 99, 271–287.
- Zarco-Tejada, P. J., Miller, J. R., Noland, T. L., Mohammed, G. H., & Sampson, P. H. (2001). Scaling-up and model inversion methods with narrow-band optical indices for chlorophyll content estimation in closed forest canopies with hyperspectral data. *IEEE Transactions on Geoscience and Remote Sensing*, 39(7), 1491–1507.
- Zlinszky, A., Mücke, W., Lehner, H., Briesche, C., & Pfeifer, N. (2012). Categorizing wetland vegetation by airborne laser scanning on Lake Balaton and Kis-Balaton, Hungary. *Remote Sensing*, 4(6), 1617–1650.
- Zlinszky, A., Tóth, V. R., Pomogyi, P., & Timár, G. (2011). Initial report of the AIMWETLAND project: Simultaneous airborne hyperspectral, LiDAR and photogrammetric survey of the full shoreline of Lake Balaton, Hungary. *Geographia Technica*, 1, 101–117.